Inorganic Chemistry

Article

pubs.acs.org/IC

Postperovskite Phase Transition of $ZnGeO_3$: Comparative Crystal Chemistry of Postperovskite Phase Transition from Germanate Perovskites

Hitoshi Yusa,*[,†] Taku Tsuchiya,[‡] Masaki Akaogi,[§] Hiroshi Kojitani,[§] Daisuke Yamazaki,[⊥] Naohisa Hirao,[∥] Yasuo Ohishi,[∥] and Takumi Kikegawa[#]

[†]National Institute for Materials Science (NIMS), 1-1, Namiki, Tsukuba, Ibaraki 305-0044, Japan

[‡]Geodynamics Research Center, Ehime University, Bunkyo-cho 2-5, Matsuyama 790-8577, Ehime Japan

[§]Department of Chemistry, Gakushuin University, 1-5-1 Mejiro, Toshima-ku, Tokyo 171-8588, Japan

[⊥]Institute for Study of the Earth's Interior, Okayama University, 827 Yamada, Misasa, Tottori 682-0193, Japan

[∥]Japan Synchrotron Radiation Research Institute (JASRI), 1-1-1 Kouto, Sayo-cho 679-5198, Japan

[#]High Energy Accelerator Research Organization (KEK), Institute of Materials Structure Science, 1-1 Oho, Tsukuba, Ibaraki 305-0801, Japan

S *Supporting Information*

ABSTRACT: The postperovskite phase of $ZnGeO_3$ was confirmed by laser heating experiments of the perovskite phase under 110−130 GPa at high temperature. Ab initio calculations indicated that the phase transition occurs at 133 GPa at 0 K. This postperovskite transition pressure is significantly higher than those reported for other germanates, such as $MnGeO_3$ and $MgGeO_3$. The comparative crystal chemistry of the perovskite-to-postperovskite transition suggests that a relatively elongated *b*-axis in the low-pressure range resulted in the delay in the transition to the postperovskite phase. Similar to most $GdFeO_3$-type perovskites that transform to the $CaIrO_3$-type postperovskite phase, $ZnGeO_3$ perovskite eventually transformed to the $CaIrO_3$-type postperovskite phase at a critical rotational angle of the GeO_6 octahedron. The formation of the postperovskite structure at a very low critical rotational angle for $MnGeO_3$ suggests that relatively large divalent cations likely break down the corner-sharing GeO_6 frameworks without a large rotation of GeO_6 to form the postperovskite phase.

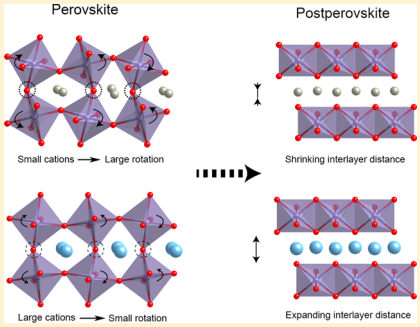

INTRODUCTION

The postperovskite phase with the $CaIrO_3$ structure has been recognized as a typical high-pressure phase of oxide and fluoride compounds since the discovery of $MgSiO_3$ postperovskite at the extreme conditions (125 GPa and 2500 K) of the lowermost part of the Earth's mantle.[1,2] Many ABO_3 compounds have been tested for transformation to the postperovskite phase in high-pressure experiments to investigate the criteria required to crystallize the $CaIrO_3$ structure. A few postperovskite phases have been found in related compounds of $CaIrO_3$ with iridium replaced by other platinum group elements, such as $CaRhO_3$,[3,4] $CaRuO_3$,[5] and $CaPtO_3$.[6,7] However, for silicates, the $ASiO_3$ end-member compositions (A = Fe, Mn, Co, and Ca) have been found not to be the $CaIrO_3$ structure.[8] Moreover, no titanates ($ATiO_3$: A = Fe, Mn, Zn, and Ca) have been reported to crystallize in the $CaIrO_3$ structure. Instead, the dissociation of $ATiO_3$ perovskite into dense compounds have been reported for $FeTiO_3$,[9,10] $MnTiO_3$,[11] $CaTiO_3$,[12] and $ZnTiO_3$.[13]

However, there are several reports of postperovskite phase transitions in germanates. The phase transitions of $MgGeO_3$[14,15] and $MnGeO_3$[16,17] have been confirmed to occur at ∼55−65 GPa by in situ high-pressure and -temperature experiments. Note that the reported transition pressures were significantly lower than that observed for $MgSiO_3$. Theoretical studies also reported phase transition pressures of 47 GPa at 0 K[18] and 51−56 GPa at 300 K[19] for $MgGeO_3$. For germanates consisting of larger divalent cations, such as $CdGeO_3$ and $CaGeO_3$, there is no agreement between theory and experiments on the postperovskite transition pressure. Although ab initio calculations predict a transition pressure of 78 GPa[18] for $CdGeO_3$, no postperovskite transition was found up to 110 GPa in laser heating experiments under high pressure.[16] Theoretical studies of $CaGeO_3$ suggest that the postperovskite transition occurs at 36 GPa,[20] 44 GPa,[20] or 55 GPa.[18] However, experimental evidence is not sufficient to confirm the theoretical results.[20]

The tendency to transform to the postperovskite phase is correlated with the orthorhombic distortion of perovskites.[8,21,22] In fact, theoretical calculations suggest that such distortion of $GdFeO_3$-type perovskite could trigger the

Received: August 15, 2014
Published: October 13, 2014

   dx.doi.org/10.1021/ic501958y | *Inorg. Chem.* 2014, 53, 11732−11739

postperovskite transition.[2] The Goldschmidt tolerance factor[23] (t) represents the orthorhombic distortion in ABO_3 perovskites: $t = (r_A + r_O)/[\sqrt{2}\,(r_B + r_O)]$, where r_A, r_B, and r_O are the ionic radii[24] of the 8-fold A cation, 6-fold B cation, and oxygen, respectively. The Goldschmidt diagram shown in Figure 1 is

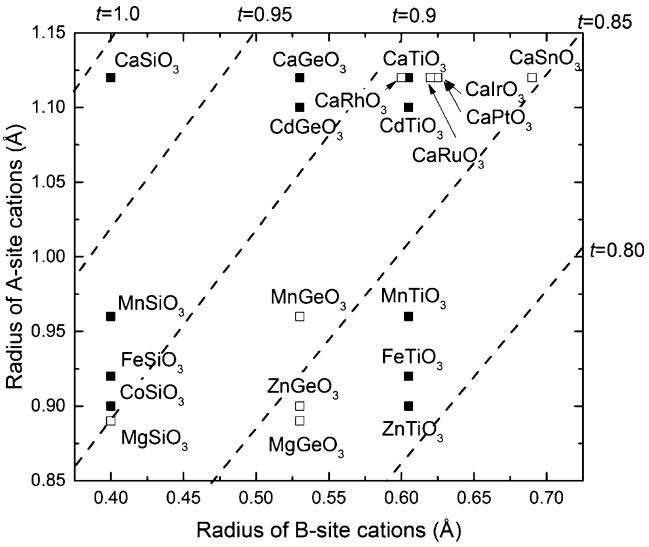

Figure 1. Goldschmidt diagram with tolerance factors of $A^{2+}B^{4+}O_3$ compounds. The tolerance factors, indicated as broken lines, were calculated from the ionic radii of the 6-fold coordinated B cations (horizontal) and 8-fold coordinated A cations (vertical). The ionic radii are from Shannon.[24] Open squares are compounds that have been confirmed to have the $CaIrO_3$-type structure. Solid squares are compounds that have not been confirmed to transform into a $CaIrO_3$-type structure. The experimental result of $CaSnO_3$ is from Tateno et al.[21]

often used to indicate the tolerance factor using both the A and B cationic radii in the perovskites. Less distorted perovskites, which give larger t, are unlikely to transform into the postperovskite phase. Indeed, germanate perovskites with large cations, such as $CaGeO_3$ (t = 0.923) and $CdGeO_3$ (t = 0.916), are not believed to transform into the $CaIrO_3$ structure because of decreasing orthorhombic distortion with increasing pressure.[16,25]

In this paper, we focus on the $ZnGeO_3$ compound to investigate the criteria for stabilizing the $CaIrO_3$ structure in germanates. Because the ionic radius of Zn^{2+} is close to that of Mg^{2+} and Mn^{2+}, the tolerance factor of $ZnGeO_3$ (t = 0.843) is close to that of $MgGeO_3$ (t = 0.835). The stable $ZnGeO_3$ perovskite structure under high pressure cannot maintain its structure during decompression and changes into a metastable $LiNbO_3$-type structure.[26] This retrogressive transformation has also been observed in $MgGeO_3$.[27] Considering the similarity of these high-pressure behaviors, the postperovskite transition also probably occurs for $ZnGeO_3$. However, the $ZnGeO_3$ postperovskite phase has not been reported. Therefore, to investigate the postperovskite transitions in $ZnGeO_3$, we first conducted in situ high-pressure X-ray diffraction (XRD) experiments combined with a laser-heated diamond anvil cell (LHDAC). Then, the phase stabilization and transition pressure were investigated by density functional theory (DFT). Additionally, XRD experiments were performed for the $MnGeO_3$ polymorphs because the lattice parameters at room temperature were not given in previous studies.[16,17] Finally, based on the crystallographic data of $AGeO_3$ (A = Ca, Cd, Mn, Zn, and Mg), we developed a comparative crystal chemistry approach for stabilizing the postperovskite phase of germanates.

EXPERIMENTAL SECTION

The ilmenite phase sample of $ZnGeO_3$ was synthesized from a mixture of ZnO and GeO_2 using a Kawai-type high-pressure apparatus at 10 GPa and 1473 K.[26] The XRD pattern of the ilmenite phase indicated that the lattice parameters (a = 4.9606[1] Å and c = 13.8645[11] Å) are in good agreement with the previously reported values.[28,29] In this product, very small amounts (less than a few percent) of GeO_2 (rutile-type) and Zn_2GeO_4 (spinel-type) compounds were also detected by XRD analysis. Two types of samples were prepared for the LHDAC experiments: one was crushed in a corundum mortar with a small amount of gold powder (~0.1 wt %) as a pressure calibrant, and another was crushed without any additives.

To prepare the starting sample of $MnGeO_3$ for the LHDAC experiments, an orthopyroxene phase was first synthesized from a mixture of MnO_2 and GeO_2 at 973 K for 20 h in air. The orthopyroxene phase was then used to synthesize $MnGeO_3$ ilmenite at 7 GPa and 1473 K for 8 h in a Kawai-type apparatus. Several of the pink single crystals (200−300 μm) were then crushed in a corundum mortar with a small amount of gold powder.

A symmetric diamond anvil cell (DAC; Syntek Co. Ltd., Yokohama, Japan) was used for the high-pressure and -temperature XRD experiments. Depending on the target pressure range, we prepared two types of diamond anvils with different culet diameters. For compression up to 78 and 135 GPa, flat anvils with a 0.3 mm diameter and beveled anvils with a 0.1 mm diameter were used, respectively. The samples were loaded into 100- to 30-μm-diameter holes in a 60- to 30-μm-thick rhenium gasket. A few ruby pressure markers (1−3 μm) were placed on the sample without the gold powder additive. The in situ XRD experiments were conducted at BL10XU (SPring-8, JASRI, Hyogo, Japan) and AR-NE1 (Photon Factory, KEK, Tsukuba, Japan). The monochromatic X-rays (30 keV) were collimated to 50−15 μm and focused on the sample in the DAC. The diffracted X-rays were detected with an imaging plate (Rigaku R-AXIS) and CCD (Bruker APEX). The Debye rings recorded on the detectors were converted into intensity versus 2θ data using the IPanalyzer program.[30] A double-sided Nd:YAG laser heating system on the beamline at BL10XU or a Nd:YLF laser at NIMS was used for the LHDAC experiments. The laser beams were focused on a 10 to 30 μm diameter spot on the sample. The temperature was monitored by measuring the gray-body radiation emitted from the sample. The laser beam scanned the sample at steps of 10 μm. We mainly collected the XRD data after laser heating because we did not observe a high-temperature phase during laser heating.

The ab initio calculations were performed using DFT[31] with the generalized gradient approximation (GGA).[32,33] Ultrasoft pseudopotentials for zinc, germanium, and oxygen were generated nonempirically using the methods of Vanderbilt.[34] The chosen plane-wave cutoff was at 50 Ry. The irreducible parts of the Brillouin zone were sampled on 4 × 4 × 4 (10 points), 4 × 4 × 4 (12 points), 4 × 4 × 2 (4 points), 4 × 4 × 2 (6 points), 4 × 4 × 4 (10 points), and 4 × 4 × 4 (4 points) Monkhorst−Pack meshes[35] for the $LiNbO_3$-type, ilmenite, orthorhombic perovskite, and $CaIrO_3$-type structures and for decomposition assemblages of ZnO (B1) and GeO_2 (pyrite-type), respectively. The structures were optimized using the variable cell-shape constant-pressure-damped molecular dynamics technique[36] using Quantum ESPRESSO[37] until the residual forces became less than 1.0×10^{-5} Ry/au. The effects of using a larger cutoff and a greater number of k points on the calculated properties were found to be insignificant.

RESULTS AND DISCUSSION

Pressure of the Perovskite-to-Postperovskite Transition of $ZnGeO_3$. In a previous study,[26] we confirmed the phase transition from $ZnGeO_3$ ilmenite to perovskite after

dx.doi.org/10.1021/ic501958y | Inorg. Chem. 2014, 53, 11732−11739

heating at 1300 K up to 31.5 GPa. In the present study, we conducted four independent LHDAC experiments at pressures higher than 35 GPa to investigate the postperovskite transition in $ZnGeO_3$. Considering the corresponding phase transition for $MnGeO_3$[16,17] and $MgGeO_3$,[14,15] we expected that the postperovskite transition would occur at ~55−65 GPa. However, no other phase apart from the perovskite phase and weak peaks from GeO_2 (pyrite structure) was observed after heating at 1600−1750 K and 97.8 GPa (Figure 2a). The

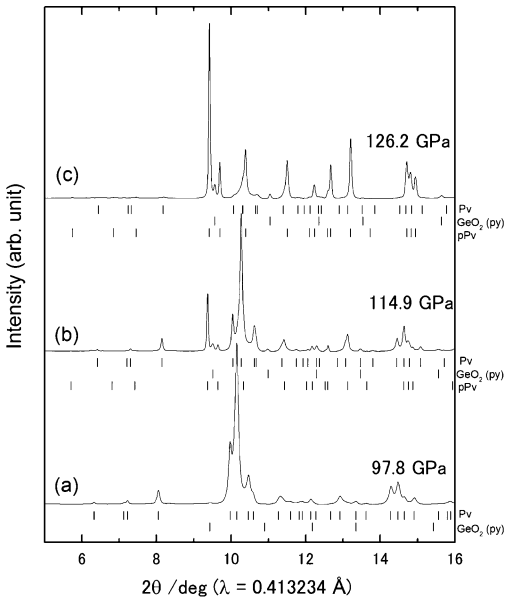

Figure 2. XRD profiles of laser-heated samples of $ZnGeO_3$ at (a) 97.8 GPa (#zg012), (b) 114.9 GPa (#zg017), and (c) 126.2 GPa (#zg024). The vertical bars represent the calculated positions of the diffraction peaks of the perovskite (Pv), postperovskite (pPv), and pyrite (GeO_2[py]) structures of GeO_2.

first sign of the postperovskite transition was observed at 114.9 GPa (Figure 2b) after heating, and the transition was almost complete after reheating at 126.2 GPa (Figure 2c). The weak peaks of GeO_2 (pyrite structure) remained after heating at 126.2 GPa. However, the 111 and 200 peaks of ZnO (rock salt structure) did not appear at 10.7° and 12.4°, respectively, where the 2θ angles were estimated from the compression study[38] of ZnO. Therefore, we concluded that the decomposition reaction into GeO_2 and ZnO, suggested by the ab initio calculation as described below, did not occur in the present high-pressure experiments. The XRD pattern was fitted to the $CaIrO_3$ structure using the LeBail method in the GSAS package program,[39] and the lattice parameters were determined to be a = 2.5742(4) Å, b = 8.2450(3) Å, and c = 6.3854(6) Å. Ruby pressure markers were used in the first LHDAC experiment. However, it was difficult to observe the ruby fluorescence above 100 GPa, probably because of the phase transition of ruby itself.[40] Because the sample did not include gold powder as a pressure calibrant, we used the lattice parameters of GeO_2, which crystallizes in the pyrite-type structure in this pressure range,[41] to determine the pressure. Further information on the pressure calibration using the lattice parameters of GeO_2 is given in the Supporting Information (Figure S1). The volume change from the perovskite phase to the postperovskite phase was calculated to be 1.6% at 114.9 GPa, where both the perovskite and postperovskite phases were observed.

To confirm the considerably higher transition pressure of $ZnGeO_3$ compared with that of $MnGeO_3$ and $MgGeO_3$, we repeated the LHDAC experiments using a sample including gold powder as a pressure calibrant.[42] All of the results of the LHDAC experiments are summarized in Table 1. The transition pressure from the LHDAC experiments was roughly determined to be 110−130 GPa at high temperatures, as shown in Figure 3.

Table 1. P−T Conditions and Phases Identified in Laser Heating Experiments

run	P_{ruby} (GPa)	P_{Au} (GPa)	$P_{GeO2-Py}$ (GPa)	T (K)	phase
zg009	62.8	NA[c]		1700 ± 100	Pv
zg012	86.0	NA[c]	97.8	1675 ± 75	Pv
zg017	NA[c]	NA[c]	114.9	2000 ± 500	Pv+pPv
zg024	NA[c]	NA[c]	126.2	2000 ± 500	pPv
zg2023	NA[c]	111.54	NA[c]	2700 ± 250	Pv
zg2032	NA[c]	130.16	NA[c]	2800 ± 300	pPv
zg2040	NA[c]	129.36	NA[c]	2500 ± 500	pPv
zg2062	NA[c]	107.89	NA[c]	2700 ± 300	Pv+pPv[a]
zg2067		107.29		3100 ± 100	Pv+pPv[a]
zg4009	NA[c]	82.1	NA[c]	3500 ± 300	Pv
zg4013	NA[c]	108.98	NA[c]	3400 ± 400	Pv
zg4016	NA[c]	117.11	NA[c]	3300 ± 100	Pv
zg4019	NA[c]	122.55	NA[c]	3700 ± 200	Pv
zg4023	NA[c]	130.79	NA[c]	2750 ± 150	Pv[b]+pPv
zg4025	NA[c]	130.89	NA[c]	2750 ± 150	Pv[b]+pPv
zg4027	NA[c]	130.14	NA[c]	3300 ± 200	Pv[b]+pPv
zg4030		135.72		3300 ± 200	Pv[b]+pPv
AG1002	NA[c]	35.0	NA[c]	NA[d]	Pv
AG1004	NA[c]	48.8	NA[c]	NA[d]	Pv
AG1006	NA[c]	60.6	NA[c]	NA[d]	Pv
AG1008	NA[c]	71.8	NA[c]	NA[d]	Pv
AG1009	NA[c]	76.1	NA[c]	NA[d]	Pv

[a]The ratio of pPv phase significantly decreased. [b]The peaks of Pv were weak but traceable. [c]The pressure calibrant was not available. [d]The sample was laser-heated but temperature was not measured.

Ab initio calculations provide useful information about the phase stability under high pressure. The relative differences in the enthalpy of perovskite-type $ZnGeO_3$ are plotted against pressure in Figure 4. The crossover point corresponding to the transformation from the ilmenite to the $CaIrO_3$-type phase at 53 GPa was not realized because of the stabilization of the perovskite phase prior to the $CaIrO_3$-type phase. The ilmenite-to-perovskite transition pressure was calculated to be 29 GPa, which is in reasonable agreement with the experimental transition pressure of 31.5 GPa.[26] The calculation clearly indicates that the perovskite phase further transformed to the postperovskite phase. The crossover point for the perovskite-to-postperovskite transition was predicted to be 133 GPa. The pressure is also much higher than the pressures determined for the postperovskite transitions of $MgGeO_3$[14,15,19] and $MnGeO_3$.[16,17] This calculation showed that the $LiNbO_3$ phase, which appeared in the retrograde transition from the perovskite phase in the previous study, seemed to be unstable. The enthalpy curve indicating the decomposition reaction into ZnO (B1) and GeO_2 (pyrite) cut across the perovskite prior to the postperovskite transition phase. However, this decomposition reaction can only be realized in a static condition

dx.doi.org/10.1021/ic501958y | Inorg. Chem. 2014, 53, 11732−11739

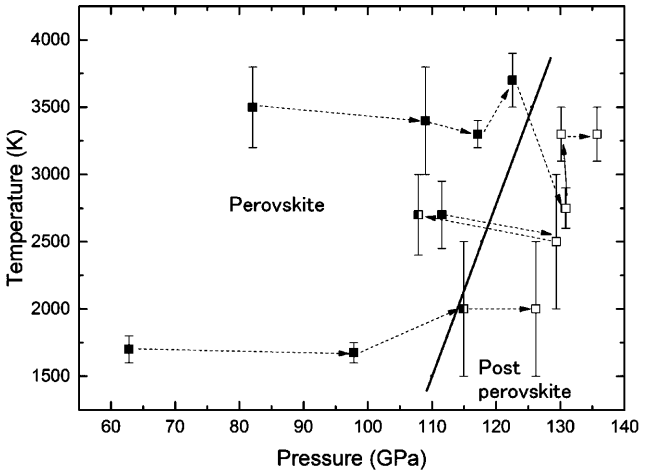

Figure 3. Estimated phase boundary between perovskite and postperovskite (solid line) from the $P-T$ conditions and the products of the LHDAC experiments (Table 1). The Clapeyron slope of +7.6 MPa/K predicted by Tsuchiya et al.[19] for $MgGeO_3$ was tentatively used to draw the phase boundary. Solid squares, open squares, and half-solid squares indicate that the products were perovskite, postperovskite, and their mixture, respectively. Dotted arrows show the path of the LHDAC experiments.

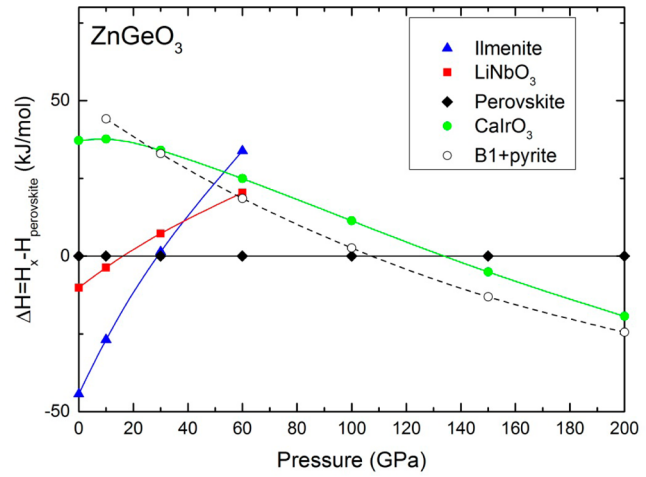

Figure 4. Enthalpy differences relative to perovskite for the ilmenite (▲), $LiNbO_3$ (■), perovskite (◆), and $CaIrO_3$ (●) phases of $ZnGeO_3$, and the decomposition reaction into ZnO (B1) plus GeO_2 (pyrite) (○) from DFT-GGA calculations.

because the $CaIrO_3$-type structure was clearly observed after sufficient annealing in the laser heating experiments.

Equation of State Parameters of $ZnGeO_3$ and $MnGeO_3$ Perovskites. To clarify the characteristics of the unusually high transition pressure for $ZnGeO_3$, we followed the compressive behavior of the perovskite phase. All of the lattice parameters collected at room temperature are shown in Table S1 of the Supporting Information, and the volumes are plotted in Figure 5. We determined the bulk modulus (K_0) of the perovskite phase by fitting the volume data to the Birch–Murnaghan equation of state and obtained K_0 = 221(5) GPa with the pressure derivative (K_0') set to 4. This value is consistent with K_0 = 216(3) GPa reported for $MgGeO_3$ perovskite.[43] However, we could not obtain a reliable value for the bulk modulus of the postperovskite phase because there

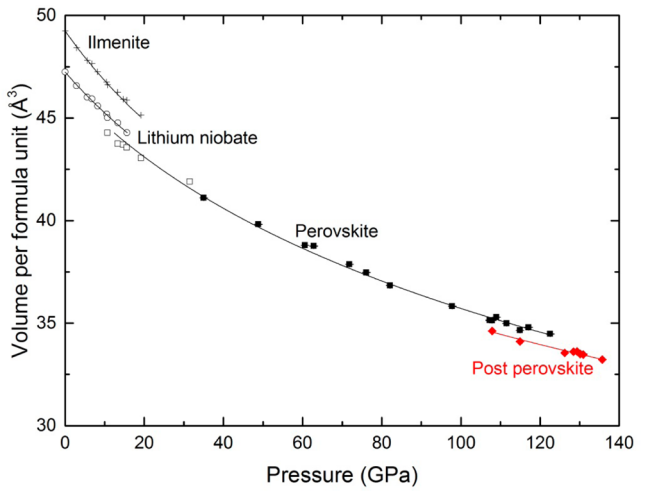

Figure 5. Compression curves and volume data of the perovskite (■) and postperovskite (◆) phases of $ZnGeO_3$. The data of ilmenite (+), lithium niobate (○), and perovskite (□) are from a previous study.[26]

are only data far away from the volume at ambient pressure (V_0).

The high-pressure behavior of $MnGeO_3$ perovskite was also investigated for comparison with the other germanate perovskites. The first appearance of the postperovskite peaks in the XRD profile (Figure 6b) was at 58.0 GPa after heating. This

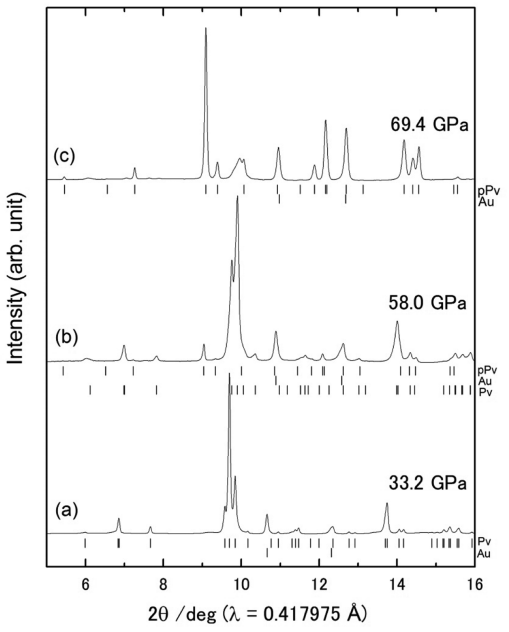

Figure 6. XRD profiles of laser-heated samples of $MnGeO_3$ at (a) 33.2, (b) 58.0, and (c) 69.4 GPa. The vertical bars represent the calculated positions of the diffraction peaks of perovskite (Pv), postperovskite (pPv), and gold (Au).

result is consistent with the high-pressure XRD study of Tateno et al.,[16] where they suggested that the postperovskite transition occurred at 58–59 GPa after laser heating. In the present study, the lattice parameters of the perovskite phase were collected in a wide pressure range. Consequently, the bulk modulus was able to be calculated: K_0 = 241(5) GPa and V_0 = 191.0(4) Å^3 with K_0' set to 4 in the Birch–Murnaghan equation of state. The volume compression curves are shown in Figure 7. The

dx.doi.org/10.1021/ic501958y | Inorg. Chem. 2014, 53, 11732–11739

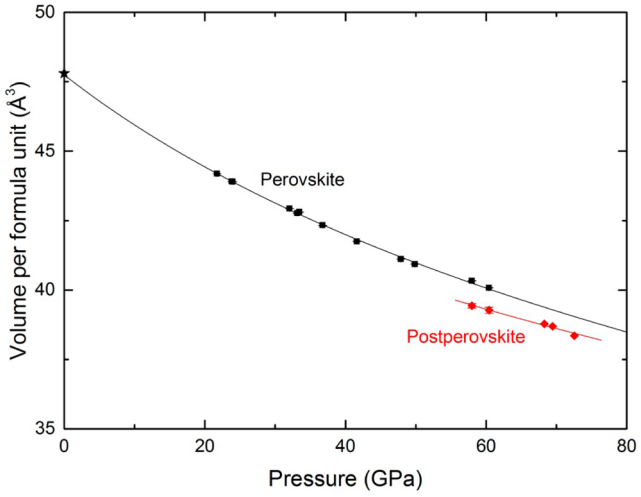

Figure 7. Compression curves and volume data of the perovskite (■) and postperovskite (◆) phases of $MnGeO_3$. The volume at atmospheric pressure (★ on the *y*-axis) was determined from the XRD profile of the recovery product.

postperovskite transition involves a volume change of 2.0–2.2%. The perovskite phase can be recovered after releasing the pressure, and then the lattice parameters are a = 5.1916(4) Å, b = 7.2832(6) Å, and c = 5.0575(8) Å, with V = 191.23(2) Å^3. All of the lattice parameters of the $MnGeO_3$ experiment are summarized in Table S2 in the Supporting Information.

High-Pressure Behavior of $AGeO_3$ (A = Zn, Mg, and Mn) Perovskites. As described above, the orthorhombic distortion in perovskite is highly related to the transformation to the postperovskite phase. To determine the orthorhombic distortion from ideal cubic perovskite, we plotted the pseudocubic unit cell parameters (i.e., $a_p = a/\sqrt{2}$, $b_p = b/2$, and $c_p = c/\sqrt{2}$ for the *Pnma* setting) and their axial ratio with pressure, which are shown in Figure 8a,b, respectively. Then, the deviation of the axial ratio from 1 indicates the degree of orthorhombic distortion in the perovskite structure. For comparison, we also performed the same data analyses for $MgGeO_3$ and $MnGeO_3$ perovskites (Figure 8c–f). The axial ratios of the $MgGeO_3$ and $MnGeO_3$ perovskites generally increased with increasing pressure. This has been suggested to be a criterion for the transition from the perovskite phase to the postperovskite phase with $CaIrO_3$ structure.[16] However, the criterion cannot be simply applied to $ZnGeO_3$ perovskite. In fact, a_p/b_p for $ZnGeO_3$ increases to 1 at 45 GPa with increasing pressure, although the other axial ratios move further away from 1 with increasing pressure. The a_p parameter becomes greater than b_p at ~45 GPa, and then the a_p/b_p ratio becomes greater than 1. This peculiar behavior is mainly because of the initial elongation of the b parameter in the low pressure range and might cause a delay of the pressure to transform into the postperovskite phase.

Relationship between Postperovskite Transition Induced by Rotation of BX_6 Octahedra and Divalent Cationic Radius. Considering the structural change from the perovskite to the postperovskite phase in ABX_3 compounds, the

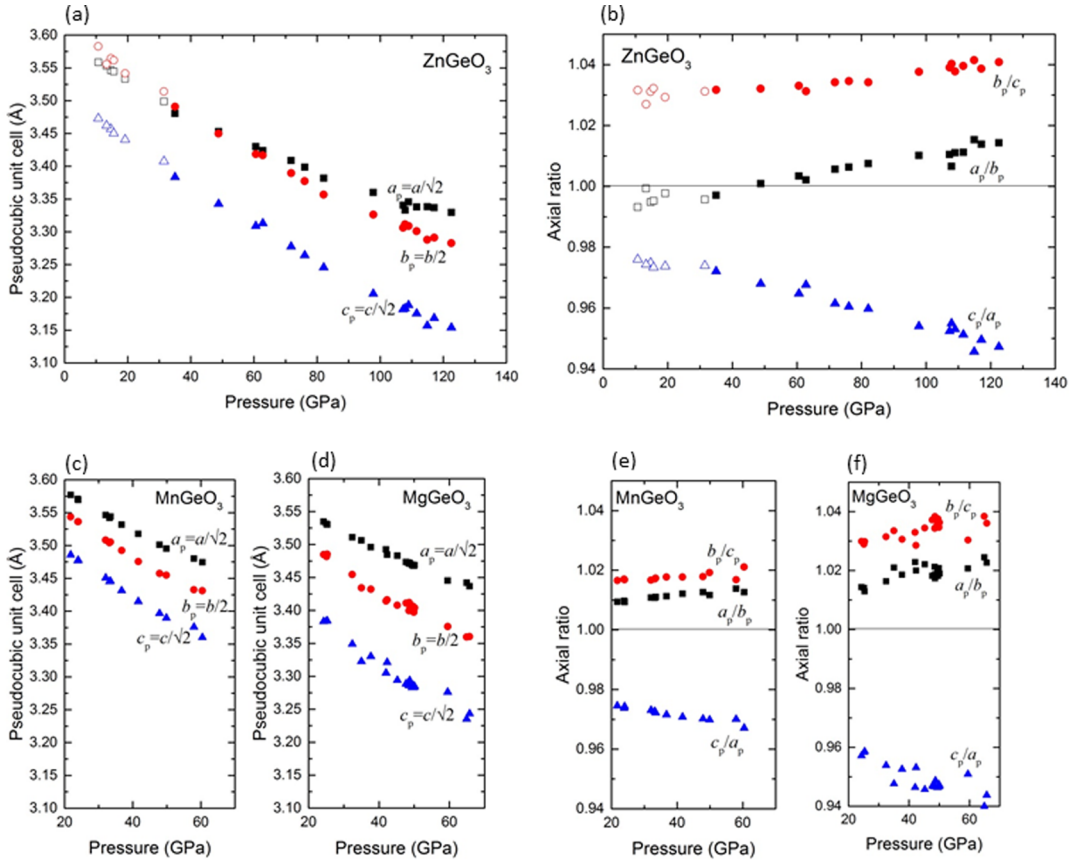

Figure 8. Pseudocubic unit cells and their axial ratios of (a, b) $ZnGeO_3$, (c, e) $MnGeO_3$, and (d, f) $MgGeO_3$. The open symbols in (a) and (b) were calculated from the data of a previous study.[26] The lattice parameter data of $MgGeO_3$ are from Runge et al.[43]

dx.doi.org/10.1021/ic501958y | Inorg. Chem. 2014, 53, 11732–11739

rotation of the BX_6 octahedra is thought to be closely related to the transformation mechanism.[2] The rotation angle (Φ) is geometrically calculated from the equation $\Phi = \cos^{-1}(\sqrt{2}c^2/ab)$,[44] where a, b, and c are the cell parameters of $GdFeO_3$-type orthorhombic perovskite (space group *Pnma*). Fujino et al.[8] and Tateno et al.[21] attempted to construct a criterion for the transformation of perovskites to the postperovskite phase based on their high-pressure experiments of oxide perovskites with $A^{2+}B^{4+}O_3$ composition, such as $CaSiO_3$, $MnSiO_3$, $MnGeO_3$, $CdGeO_3$, and $CaSnO_3$. The criterion is as follows: for the postperovskite transition, it is necessary that the orthorhombic distortion increases with pressure; otherwise, the transition never occurs. In other words, Φ reaches a critical angle, and then the postperovskite phase forms. Tateno et al.[21] suggested that the postperovskite transition in oxide perovskites mostly occurs at $\sim\Phi = 25°$. Recent compression studies of fluoride perovskites with $Na^+B^{2+}F_3$ composition, such as $NaMgF_3$,[45] $NaCoF_3$,[22] $NaNiF_3$,[22] and $NaZnF_3$,[46] indicated that the transition started at $\Phi = 24–27°$. Therefore, to confirm the validity of the transition pressure of $ZnGeO_3$, it is necessary to investigate the pressure variation of Φ in $ZnGeO_3$ perovskite. In the low-pressure range considered in a previous study, the change of Φ with pressure was too small to assess the relationship between Φ and the phase transition. However, the current study performed for a higher pressure region clearly shows that Φ increases with increasing pressure and reaches 24° at the transition pressure (Figure 9). Therefore, $ZnGeO_3$ almost agrees with the criterion mentioned above. To compare Φ of the various germanates with different divalent cations, the variation of Φ with pressure for $MgGeO_3$ and $MnGeO_3$ are also plotted in Figure 9. The gradient of Φ is almost independent of the divalent cation species. However, note that the Φ value at the transition pressure (Φ_{tr}) for $MnGeO_3$ is very low (Φ_{tr} = 18°) compared with the values of other compounds. The ionic radius of Mn^{2+} (0.96 Å) is significantly larger than that of Mg^{2+} (0.89 Å) and Zn^{2+} (0.90 Å). Therefore, the low Φ_{tr} value for $MnGeO_3$ suggests that the $CaIrO_3$-type postperovskite phase crystallizes with the large divalent cation suppressing the rotation of GeO_6 octahedra in the perovskite structure. In fact, there is a correlation between Φ_{tr} and the divalent cationic radius (Figure 9b). Therefore, in the perovskites with large divalent cations, the corner-sharing GeO_6 frameworks could not retain sufficient space to incorporating the cations by increasing the tilting angle. These frameworks likely break down to form the postperovskite structure without a large rotation of GeO_6 octahedra. The scheme for the transformation is illustrated in Figure 10.

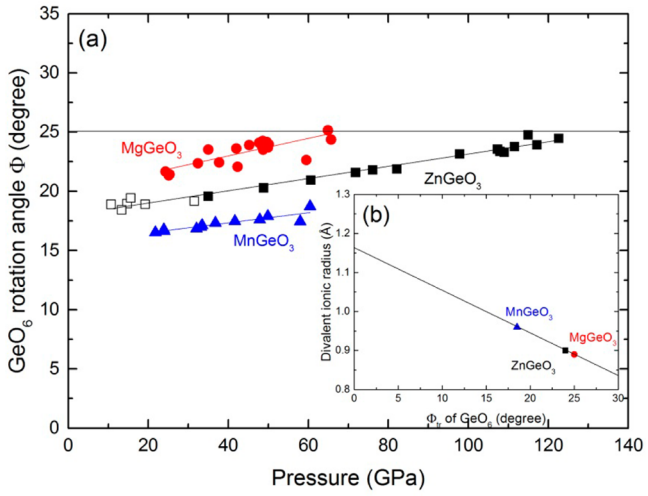

Figure 9. (a) GeO_6 rotation angle (Φ) in perovskites as a function of pressure. Circles, squares, and triangles represent the Φ values of $MgGeO_3$, $ZnGeO_3$, and $MnGeO_3$, respectively. The lattice parameters used to calculate Φ of $MgGeO_3$ were from Runge et al.[43] Open squares are from a previous study.[26] (b) Relationship between Φ_{tr} and the divalent cationic radii of $MgGeO_3$, $ZnGeO_3$, and $MnGeO_3$.

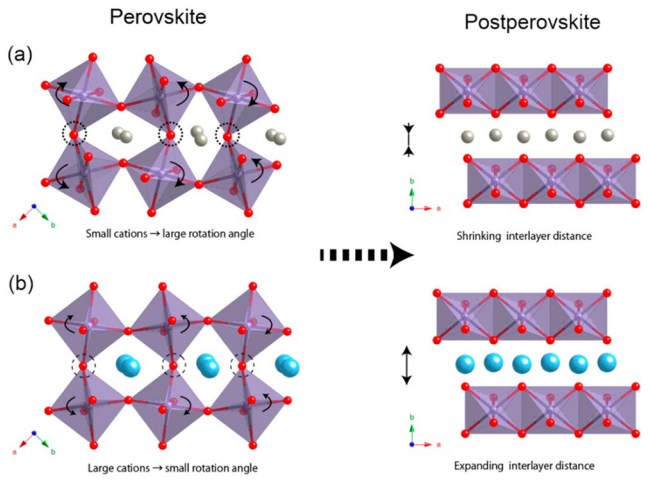

Figure 10. Schematic illustrations of the phase transition from the perovskite to the postperovskite phase consisting of (a) small A site cations and (b) large A site cations. Dotted circles show the breakdown points of corner-sharing GeO_6 during the phase transformation.

According to the geometry of the $CaIrO_3$ structure, divalent cations incorporate into the GeO_6 layered structure perpendicular to the *b*-axis. Therefore, the *b*-axis should be the most sensitive to the divalent cationic radius. In fact, the *b*-axis of $MnGeO_3$ is considerably longer than those of other germanates, as shown in Figure 11. This can be attributed to the ability of the $CaIrO_3$ structure to incorporate large divalent cations.

Postperovskite Transition in Germanate Perovskites Containing Large Divalent Cations. Investigation of the germanate postperovskites containing divalent cations larger than Mn^{2+} (0.96 Å), such as $CdGeO_3$ and $CaGeO_3$, is not complete. Wu et al.[20] detected an XRD peak corresponding to the postperovskite phase of $CaGeO_3$ at 43 GPa, although they did not report the lattice parameters of postperovskite. We calculated Φ from their reported perovskite lattice parameters and found that Φ exhibited abnormal behavior with increasing pressure as shown in Figure S2 of the Supporting Information. Less distorted orthorhombic lattices, such as $CdGeO_3$ and $CaGeO_3$ perovskites, tend to affect the accuracy of the *d*-values because of the difficulty in the peak-fitting analysis of multiple overlapping peaks (e.g., 200, 121, and 002 for the *Pnma* setting). Therefore, the inaccurate lattice parameters of the perovskite phase probably make it difficult to discuss the relationship between the postperovskite transitions with Φ. A high-pressure X-ray single-crystal study of $CaGeO_3$ up to 8.5 GPa indicated that Φ decreased with increasing pressure.[25] This is in agreement with the tendency of the perovskite phase to move toward the ideal cubic perovskite structure.

dx.doi.org/10.1021/ic501958y | *Inorg. Chem.* 2014, 53, 11732–11739

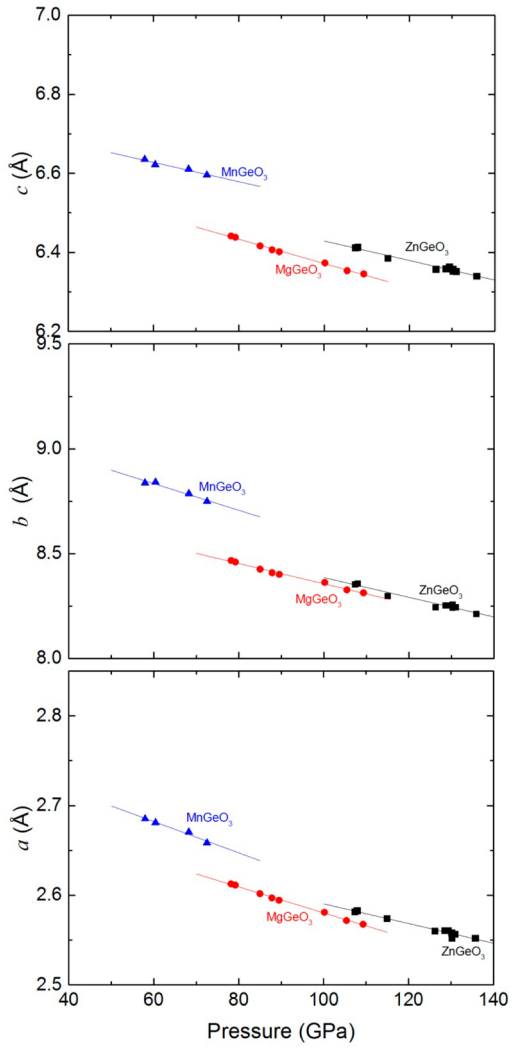

Figure 11. Comparison of the lattice parameters of various postperovskite phases as a function of pressure. Triangles, squares, and circles represent the lattice parameters of $MnGeO_3$, $ZnGeO_3$, and $MgGeO_3$, respectively. The lattice parameters of $MgGeO_3$ are from Kubo et al.[47]

In situ XRD experiments of $CdGeO_3$ have been reported by Tateno et al.[16] They reported that the Φ value decreased with increasing pressure and finally reached a value close to 0° at 55 GPa. Consequently, the postperovskite transition is unlikely to occur in $CdGeO_3$ because the rotation of GeO_6 is to the opposite side of the orthorhombic distortion. Thus, we can conclude that the postperovskite transition does not occur in germanate perovskites containing divalent cations larger than Cd^{2+}. However, further high-pressure XRD experiments should be performed for both $CaGeO_3$ and $CdGeO_3$ perovskites up to much higher pressure to confirm that the postperovskite transition does not occur.

SUMMARY

The postperovskite phase of $ZnGeO_3$ with the $CaIrO_3$ structure was observed above 115 GPa after laser heating the sample. Although the transition pressure was considerably higher than the corresponding pressures for other germanate postperovskite transitions, the transition pressure was consistent with the theoretical result. The orthorhombic distortion indicator (Φ) of $ZnGeO_3$ perovskite gradually increased with increasing pressure and reached 24° at the transition pressure, which is in agreement with many other perovskite−postperovskite transitions of ABX_3 compounds. The very low Φ_{tr} value in $MnGeO_3$ suggests that the corner-sharing GeO_6 frameworks could not retain sufficient space to incorporate the large divalent cations by increasing the tilting angle. This could also contribute to the ability of the postperovskite structure to incorporate large divalent cations. Germanate perovskites incorporating divalent cations larger than Cd^{2+} cannot crystallize in the $CaIrO_3$ structure because increasing the pressure does not promote octahedral rotation to induce the postperovskite transition.

ASSOCIATED CONTENT

Supporting Information

Pressure calibration using linear compressibility of GeO_2 pyrite phase, lattice parameters of perovskite and postperovskite phases, and comparison of Φ of $CdGeO_3$ and $CaGeO_3$ perovskites with $MnGeO_3$, $ZnGeO_3$, and $MgGeO_3$ perovskites. This material is available free of charge via the Internet at http://pubs.acs.org.

AUTHOR INFORMATION

Corresponding Author

*E-mail: yusa.hitoshi@nims.go.jp.

Notes

The authors declare no competing financial interest.

ACKNOWLEDGMENTS

The synchrotron radiation experiments were conducted at BL10XU in SPirng-8, and at AR-NE1 in Photon Factory (KEK) with the approval of JASRI (Proposal Nos. 2012B1186 and 2012B1187) and KEK (Proposal No. 2013G590). This work was supported by JSPS KAKENHI (Grant Nos. 24654177 and 25106006).

REFERENCES

(1) Murakami, M.; Hirose, K.; Kawamura, K.; Sata, N.; Ohishi, Y. *Science* **2004**, *304*, 855−858.
(2) Tsuchiya, T.; Tsuchiya, J.; Umemoto, K.; Wentzcovitch, R. M. *Earth Planet. Sci. Lett.* **2004**, *224*, 241−248.
(3) Shirako, Y.; Kojitani, H.; Akaogi, M.; Yamaura, K.; Takayama-Muromachi, E. *Phys. Chem. Miner.* **2009**, *36*, 455−462.
(4) Yamaura, K.; Shirako, Y.; Kojitani, H.; Arai, M.; Young, D. P.; Akaogi, M.; Nakashima, M.; Katsumata, T.; Inaguma, Y.; Takayama-Muromachi, E. *J. Am. Chem. Soc.* **2009**, *131*, 2722−2726.
(5) Kojitani, H.; Shirako, Y.; Akaogi, M. *Phys. Earth Planet. Inter.* **2007**, *165*, 127−134.
(6) Inaguma, Y.; Hasumi, K.; Yoshida, M.; Ohba, T.; Katsumata, T. *Inorg. Chem.* **2008**, *47*, 1868−1870.
(7) Ohgushi, K.; Matsushita, Y.; Miyajima, N.; Katsuya, Y.; Tanaka, M.; Izumi, F.; Gotou, H.; Ueda, Y.; Yagi, T. *Phys. Chem. Miner.* **2008**, *35*, 189−195.
(8) Fujino, K.; Nishio-Hamane, D.; Suzuki, K.; Izumi, H.; Seto, Y.; Nagai, T. *Phys. Earth Planet. Inter.* **2009**, *177*, 147−151.
(9) Nishio-Hamane, D.; Yagi, T.; Ohshiro, M.; Niwa, K.; Okada, T.; Seto, Y. *Phys. Rev. B* **2010**, *82*, 092103.
(10) Nishio-Hamane, D.; Zhang, M. G.; Yagi, T.; Ma, Y. M. *Am. Mineral.* **2012**, *97*, 568−572.
(11) Okada, T.; Yagi, T.; Nishio-Hamane, D. *Phys. Chem. Miner.* **2011**, *38*, 251−258.
(12) Hamane, D.; Yagi, T. *Rev. High Pressure Sci. Technol.* **2012**, *22*, 246.

(13) Akaogi, M.; Abe, K.; Yusa, H.; Kojitani, H.; Mori, D.; Inaguma, Y. *Phys. Chem. Miner.* To be submitted.
(14) Hirose, K.; Kawamura, K.; Ohishi, Y.; Tateno, S.; Sata, N. *Am. Mineral.* **2005**, *90*, 262−265.
(15) Ito, E.; Yamazaki, D.; Yoshino, T.; Fukui, H.; Zhai, S. M.; Shatzkiy, A.; Katsura, T.; Tange, Y.; Funakoshi, K. *Earth Planet. Sci. Lett.* **2010**, *293*, 84−89.
(16) Tateno, S.; Hirose, K.; Sata, N.; Ohishi, Y. *Phys. Chem. Miner.* **2006**, *32*, 721−725.
(17) Yamazaki, D.; Ito, E.; Katsura, T.; Yoshino, T.; Zhai, S. M.; Fukui, H.; Shatskiy, A.; Guo, X. Z.; Shan, S. M.; Okuchi, T.; Tange, Y.; Higo, Y.; Funakoshi, K. *Am. Mineral.* **2011**, *96*, 89−92.
(18) Fang, C. M.; Ahuja, R. *Phys. Earth Planet. Inter.* **2006**, *157*, 1−7.
(19) Tsuchiya, T.; Tsuchiya, J. *Phys. Rev. B* **2007**, *76*, 092105.
(20) Wu, X.; Qin, S.; Gu, T.-T.; Yang, J.; Manthilake, G. *Phys. Earth Planet. Inter.* **2011**, *189*, 151−156.
(21) Tateno, S.; Hirose, K.; Sata, N.; Ohishi, Y. *Phys. Earth Planet. Inter.* **2010**, *181*, 54−59.
(22) Yusa, H.; Shirako, Y.; Akaogi, M.; Kojitani, H.; Hirao, N.; Ohishi, Y.; Kikegawa, T. *Inorg. Chem.* **2012**, *51*, 6559−6566.
(23) Goldschmidt, V. M. *Naturwissenschaften* **1926**, *14*, 477−485.
(24) Shannon, R. D. *Acta Crystallogr., Sect. A* **1976**, *32*, 751−767.
(25) Ross, N. L.; Angel, R. J. *Am. Mineral.* **1999**, *84*, 277−281.
(26) Yusa, H.; Akaogi, M.; Sata, N.; Kojitani, H.; Yamamoto, R.; Ohishi, Y. *Phys. Chem. Miner.* **2006**, *33*, 217−226.
(27) Leinenweber, K.; Wang, Y. B.; Yagi, T.; Yusa, H. *Am. Mineral.* **1994**, *79*, 197−199.
(28) Syono, Y.; Akimoto, S. I.; Matsui, Y. *J. Solid State Chem.* **1971**, *3*, 369−380.
(29) Ross, N. L.; Leinenweber, K. *Z. Kristallogr.* **1990**, *191*, 93−104.
(30) Seto, Y.; Nishio-Hamane, D.; Nagai, T.; Sata, N. *Rev. High Pressure Sci. Technol.* **2010**, *20*, 269−276.
(31) Hohenberg, P.; Kohn, W. *Phys. Rev. B* **1964**, *136*, B864−871.
(32) Ceperley, D. M.; Alder, B. J. *Phys. Rev. Lett.* **1980**, *45*, 566−569.
(33) Perdew, J. P.; Zunger, A. *Phys. Rev. B* **1981**, *23*, 5048−5079.
(34) Vanderbilt, D. *Phys. Rev. B* **1990**, *41*, 7892−7895.
(35) Monkhorst, H. J.; Pack, J. D. *Phys. Rev. B* **1976**, *13*, 5188−5192.
(36) Wentzcovitch, R. M. *Phys. Rev. B* **1991**, *44*, 2358−2361.
(37) Baroni, S.; de Gironcoli, S.; Dal Corso, A.; Giannozzi, P. *Rev. Mod. Phys.* **2001**, *73*, 515−562.
(38) Liu, H.; Tse, J. S.; Mao, H.-k. *J. Appl. Phys.* **2006**, *100*, 093509.
(39) Larson, A. C.; Von Dreele, R. B. *Los Alamos National Laboratory Report LAUR* **2004**, 86−748.
(40) Lin, J. F.; Degtyareva, O.; Prewitt, C. T.; Dera, P.; Sata, N.; Gregoryanz, E.; Mao, H. K.; Hemley, R. J. *Nat. Mater.* **2004**, *3*, 389−393.
(41) Ono, S.; Tsuchiya, T.; Hirose, K.; Ohishi, Y. *Phys. Rev. B* **2003**, *68*, 014103.
(42) Anderson, O. L.; Isaak, D. G.; Yamamoto, S. *J. Appl. Phys.* **1989**, *65*, 1534−1543.
(43) Runge, C. E.; Kubo, A.; Kiefer, B.; Meng, Y.; Prakapenka, V. B.; Shen, G.; Cava, R. J.; Duffy, T. S. *Phys. Chem. Miner.* **2006**, *33*, 699−709.
(44) O'keeffe, M.; Hyde, B. G.; Bovin, J. O. *Phys. Chem. Miner.* **1979**, *4*, 299−305.
(45) Martin, C. D.; Crichton, W. A.; Liu, H. Z.; Prakapenka, V.; Chen, J. H.; Parise, J. B. *Geophys. Res. Lett.* **2006**, *33*, L11305.
(46) Yakovlev, S.; Avdeev, M.; Mezouar, M. *J. Solid State Chem.* **2009**, *182*, 1545−1549.
(47) Kubo, A.; Kiefer, B.; Shim, S. H.; Shen, G.; Prakapenka, V. B.; Duffy, T. S. *Am. Mineral.* **2008**, *93*, 965−976.